

## Quasi-Stationary Waves in the Southern Hemisphere. Part II: Generation Mechanisms

ARTURO I. QUINTANAR AND CARLOS R. MECHOSO

*Department of Atmospheric Sciences, University of California at Los Angeles, Los Angeles, California*

(Manuscript received 18 August 1994, in final form 23 March 1995)

### ABSTRACT

In this Part II the authors investigate the role that Antarctic elevations, the rest of the world orography, thermal forcing from lower latitudes, and the transient eddy component of the flow play on the generation of the quasi-stationary wave field in the Southern Hemisphere. An approach based on the UCLA GCM is followed. Results from a control simulation with full orography and from experiments without the Antarctic elevations and without the rest of the world orography, suggest that the quasi-stationary wave with zonal wavenumber 1 (QS-wave 1) around Antarctica is primarily generated by mechanisms other than the Antarctic elevations.

Comparison of a three-dimensional Eliassen–Palm flux vector in the control simulation, and those where the Antarctic elevation and the rest of the world orography are removed, suggests that wave activity propagates both from the subtropics and from polar latitudes. Although in qualitative agreement with results of Part I, the horizontal and vertical structure of these remote forcings is different in the simulations where a more barotropic wave train is generated from lower and polar latitudes. Antarctica is indeed a source of wave activity but unlike observations it is confined to polar regions at tropospheric levels. Additional evidence of thermal forcing was found in an experiment without orographic elevations and zonal asymmetries south of 45°S. It is found that QS-wave 2 is most affected by the zonal asymmetries in sea ice and SST.

The effects of the transient component of the flow were also analyzed. The heat transport by the transient eddies in the absence of Antarctic elevations is greater than in the control simulation consistent with a warming of the polar region. Analysis of the contribution by the low-pass and high-pass transients to QS-wave 1 in the control simulation reveals a very different behavior than in Part I. In the control simulation, the low-pass transients and QS-wave 1 are mostly in opposition of phase. High-frequency transients are uncorrelated with QS-wave 1 in all cases. In the experiments without Antarctic elevations or the rest of the world orography, low-pass transients are in phase with QS-wave 1 over high and polar latitudes. In summary, the results of this study suggest that the generation of QS-wave 1 at high latitudes is predominantly from lower latitudes.

### 1. Introduction

Identification of the generation mechanisms for the quasi-stationary wave field in the troposphere and stratosphere is a long standing issue in dynamic meteorology and climatology. A long line of research on the subject was initiated by Charney and Eliassen's (1949) paper on the stationary response associated with orography, and by Smagorinsky's (1953) study on the effects of a middle-latitude heat source on the generation of the quasi-stationary wave field (see reviews by Smith 1979; Dickinson 1980; Kasahara 1980). Most of that research emphasized orographic and thermal forcings corresponding to the Northern Hemisphere.

Relatively few studies specifically address the generation mechanisms of quasi-stationary waves in the Southern Hemisphere. James (1988) used a model based on the barotropic vorticity equation linearized

about the zonally symmetric winter mean vorticity at 300 mb. He found that both idealized and realistic representations of the Antarctic elevations forced a stationary wave pattern that propagated into middle latitudes. Quintanar and Mechoso (1989) computed the stationary solutions of a nonlinear barotropic model for orographic distributions consisting only of either idealized or realistic representations of the Antarctica orography. The structure of these solutions showed substantial similarities with the observed quasi-stationary wave field in the Southern Hemisphere when the flow is relaxed to a zonally symmetric velocity profile corresponding to the winter climatology. Watterson and James (1992) analyzed the stationary response of the flow to a circular dome of 3000 m height centered 10° in latitude off the southern pole. They used two versions of a hemispheric, 10-layer, primitive equation model: 1) a version linearized about a zonally symmetric zonal wind distribution compiled from a winter climatology, and 2) a "semilinear" version, in which the same zonally symmetric zonal wind distribution was kept unchanged during the model's integration. Thus, wave–wave interactions were allowed in this version. The results obtained with the linear version

---

*Corresponding author address:* Dr. Arturo I. Quintanar, Centro de Ciencias de la Atmosfera, Circuito Exterior, Ciudad Universitaria, C.P. 04510 Mexico D.F., Mexico.

showed largest values of zonally asymmetric relative vorticity in the polar region with weak values at high and midlatitudes. The results obtained with the semilinear version also showed largest values in the polar latitudes, but produced significant values at high and middle latitudes. Watterson and James (1992) concluded that the Antarctic orography is capable of forcing a significant quasi-stationary wave field in the southern middle and high latitudes, and suggested that the flow transients can play a significant role in the generation of quasi-stationary features of the flow.

There is a substantial body of literature on the sensitivity of the circulation simulated with GCMs to the distribution of orography. Although most of these studies were performed in the global domain, relatively little attention has been given to the results for the Southern Hemisphere. This was partly due to the generally poor GCM performance in the high southern latitudes, which are characterized by a strong—but difficult to simulate—semipermanent trough around Antarctica (e.g., Jenne et al. 1974). Mechoso (1981) compared July simulations using a version of the NOAA/Princeton University Geophysical Fluid Dynamics Laboratory (GFDL) GCM with and without surface elevations. Unlike its predecessors, this version of the GFDL GCM produced a realistic simulation of the sub-Antarctic trough. Mechoso (1981) found significant differences between the amplitude and meridional structure of the quasi-stationary waves obtained in the simulations. He discussed the contribution of Antarctica to the existence of very cold temperatures over the polar regions. In his scenario, the transport of heat by transient eddies to the southern polar region is weak since the constraints imposed by the Antarctic elevations on the trajectories of cyclones prevent their migration onto the continent. Another factor to consider is the radiational cooling by the elevated Antarctic surfaces. Simmonds and Lin (1983) investigated the role of orography and sea surface temperature (SST) distributions on the Southern Hemisphere circulation by using a hemispheric version of the Melbourne University GCM in the perpetual-January mode. This GCM simulated a realistic sub-Antarctic trough and subtropical highs but failed to obtain the strong westerlies observed between 40° and 60°S at 500 mb. In addition, the simulated amplitude of the time-mean component of the geopotential height field at 500 mb with zonal wavenumber 1 (QS-wave 1) was about 80% of that observed at middle and high latitudes. Simmonds and Lin (1983) found that orography does not significantly affect the location of the subtropical highs; the effect of sea-land temperature contrasts were more important in this respect. The amplitude of QS-wave 1 did not change significantly when either the Antarctic elevations or all orographic elevations were excluded from the model's boundary conditions. Tokioka and Noda (1986) carried out simulations using the six-layer version of the Meteorological Research Institute (MRI) GCM in the perpetual-

January mode with different orographic distributions. As in Held (1983), they called "orographic component" of the response to the difference between the results obtained with and without orography, and "thermal component" of the response to the fields obtained without orography. In the upper troposphere of the Northern Hemisphere, Tokioka and Noda (1986) found that orographic and thermal components had similar magnitude. In the Southern Hemisphere, on the other hand, the orographic component, which was dominated by QS-wave 1, was substantially weaker than the thermal component. They also found that removal of the mountains results in a cooling of the north polar regions, and a warming of the south polar regions.

The consensus view, therefore, is that substantial progress in the understanding of the generation mechanisms of quasi-stationary waves has been made since the seminal works of Charney and Smagorinsky in the 1950s. The Southern Hemisphere, however, adds special challenges to the problem. These challenges result from the presence of an elevated and perpetually ice-covered continent in the polar region, but not centered at the pole. Antarctica is primarily inside the polar vortex where potential vorticity gradients are weak and nonlocal connections are difficult to explain from a dynamical viewpoint. Part II of this two-part paper addresses these challenges by using the UCLA GCM. The focus is on three basic questions.

1) *What is the sensitivity of the simulated quasi-stationary wave field to orographic elevations, particularly those of Antarctica?*

2) *What is the relative importance of orographic forcing, thermal forcing from lower latitudes and zonal asymmetries in surface conditions other than orography (i.e., SST and sea ice) in determining the structure of the quasi-stationary wave field at middle and high latitudes?*

3) *How does orography affect the distribution of transient eddy fluxes and in turn affect the quasi-stationary wave field?*

This Part II is organized as follows. Section 2 describes the control simulation and hypothesis-testing experiments performed with the GCM. Section 3 discusses the effects that different surface boundary conditions have on the simulated quasi-stationary geopotential height and temperature fields of the Southern Hemisphere. The simulated propagation of quasi-stationary planetary waves and the effects of transient eddies on the time-mean flow are examined in sections 4 and 5, respectively. The conclusions of the study are presented in section 6. A brief description of the UCLA GCM is given in appendix A.

## 2. Control simulation

Our control simulation (CTRL) consists of a 225-day integration in the perpetual-October mode (i.e., the

insolation is fixed at its value for mid-October, and the prescribed geographical distributions of surface conditions correspond to the October climatology). (The length of CTRL represents a compromise between the period of simulation required to obtain reasonably stable statistics and the available computer resources.) October is chosen since the amplitude of QS-wave 1 in the southern stratosphere is maximum during the austral fall (see Part I). To compute time means and standard deviations we define an ensemble of five 30-day periods separated by 15-day intervals. We performed a Student t-test to estimate the statistical significance of our results. The results of this test are not included in this paper. Suffice to say, the most notable features that will be discussed in this study are statistically significant at the 90% level. In the following presentation, the latitudinal belts 30°–50°S, 50°–70°S, and 70°–90°S will be referred to as the middle, high, and polar latitudes, respectively.

We first present selected results obtained in CTRL. Figure 1 shows the time-mean zonally asymmetric component of the geopotential and temperature fields at 300 mb. The simulated geopotential height is very similar to the observed (see Fig. 1 in Part I) except for somewhat weaker amplitudes and a slight westward shift in the position of the negative center. At middle latitudes, the region of positive values extends from the east coast of South America to the date line with an absolute maximum of about 50 m just west of South Africa. The region of negative values extends from about 160°W with a maximum of about 50 m over the central Pacific Ocean. In the high and polar latitudes, the simulated fields are clearly dominated by QS-wave

1. For the geopotential height, the largest magnitudes are in high latitudes with local maxima of about 80 m near the west coast of South America and of about 60 m over the central Pacific. A region of negative values extends from the east coast of South America to the Indian Ocean, with largest magnitudes of about 120 m over Africa. At polar latitudes, there is a prominent low center near 120°E with an amplitude of about 60 m. The location of this center is slightly west of the observed.

The temperature field at middle latitudes shows temperatures about 2°C warmer than the zonal mean over the west coasts of South Africa and Australia and colder by about 1°C over the eastern Pacific Ocean (see Fig. 2 in Part I). At high latitudes there are warmer temperatures (of about 1°C) west of the Antarctic peninsula, and colder temperatures (of about 1°C) in the South Atlantic sector. A maximum value of about 1.5°C is found over the Greenwich meridian. At polar latitudes, colder temperatures (of about 1°C) are over East Antarctica and warmer temperatures over West Antarctica, as observed.

Figure 2 shows QS-wave 1 in geopotential height at 300 mb for October and that simulated in CTRL. The largest amplitudes of QS-wave 1 in CTRL and those obtained from observational data are between 50° and 60°S, where the phases differ by about 30°. The maximum amplitude in CTRL is about 10% smaller than the observed (see also Fig. 7). The phases of simulated and observed QS-wave 1 at polar latitudes are almost in quadrature. In particular, the low centers are over the date line in the observational data and over East Antarctica in CTRL.

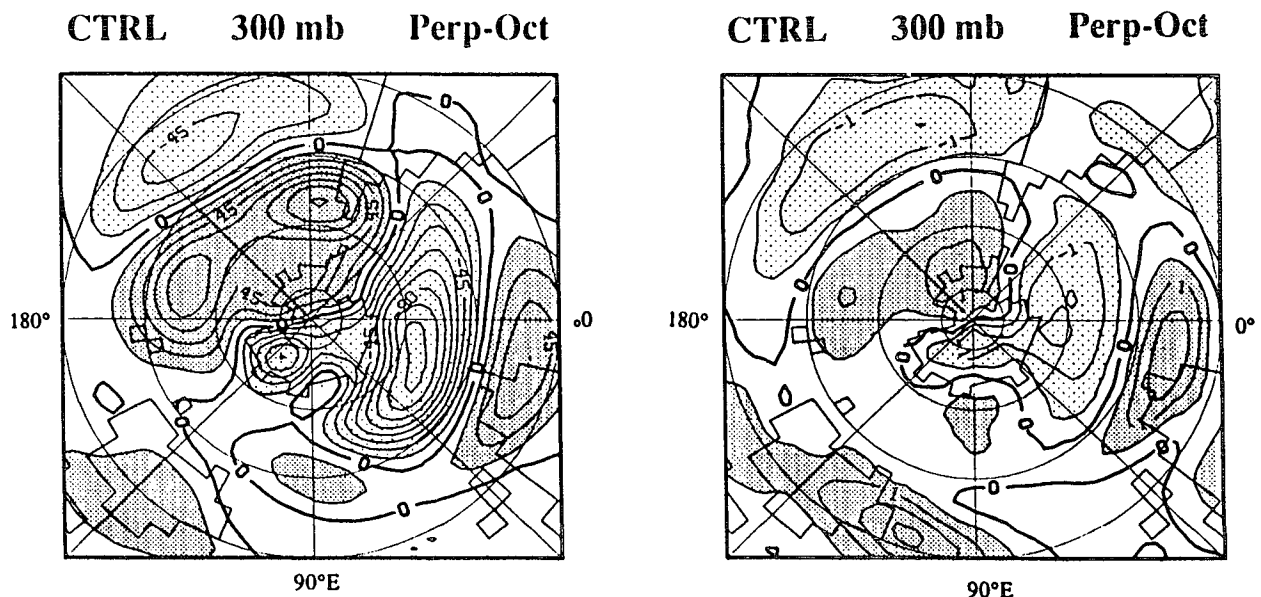


FIG. 1. The 300-mb time-mean zonal asymmetries in the control simulation (CTRL) of geopotential height (left) and temperature (right). Dark and light shading correspond to positive and negative values, respectively. The contour intervals are 15 m and 0.5 K, respectively.

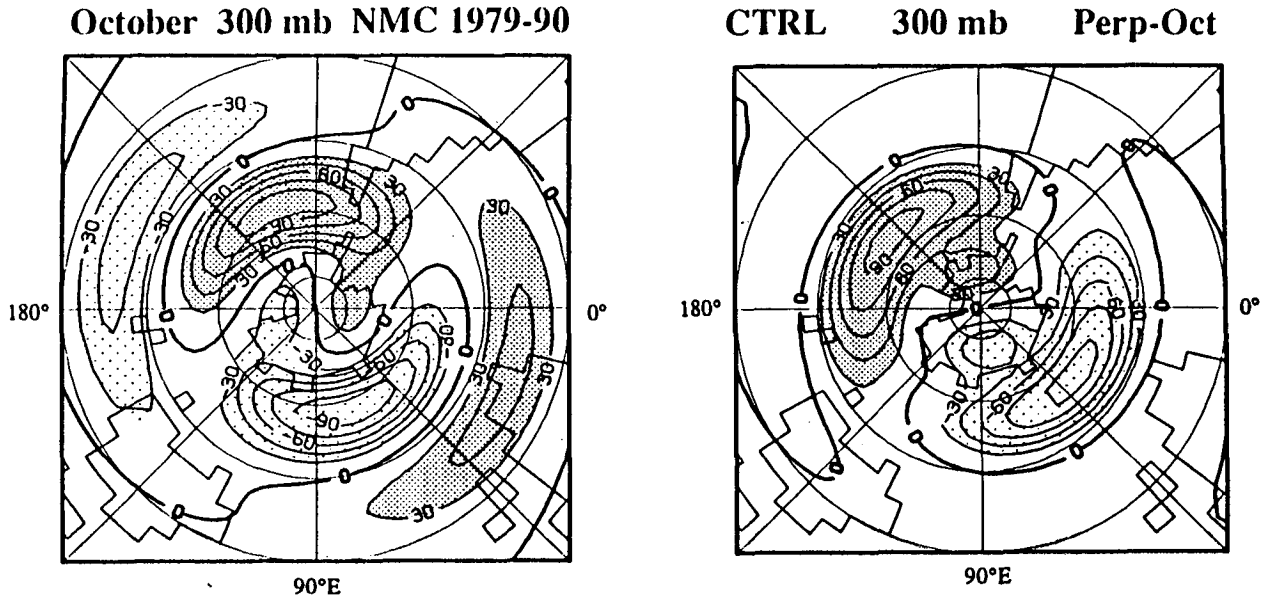


FIG. 2. QS-wave 1 geopotential height at 300 mb for October (left) and for the control (CTRL) simulation (right). Contour interval is 15 m.

Figure 3 shows longitude–height cross sections of the zonally asymmetric component of geopotential height at 55°S and 75°S. At 75°S, there is a shallow layer with geopotential height higher than the zonal mean (i.e., anticyclonic vorticity) over the surface of Antarctica. Immediately above this surface layer there is cyclonic vorticity. This structure was associated in Part I to the strong cooling from the Antarctic surface (see Figs. 4 and 5 in Part I). The similarity between the quasi-stationary wave field at polar latitudes simulated in CTRL and the observed suggests that a mechanism similar to the drainage winds operates in the

GCM. In fact, close to the Antarctic surface (about 600 mb) over most of Antarctica there are weak easterly winds (about  $1 \text{ m s}^{-1}$  over the plateau to about  $3 \text{ m s}^{-1}$  over the Antarctic periphery) (not shown). This implies that a weak meridional direct circulation must be generated in the CTRL simulation.

The corresponding plots for QS-wave 1 are shown in Fig. 4. It is obvious that QS-wave 1 dominates in the lower troposphere at high and polar latitudes. At high latitudes in the upper troposphere and stratosphere QS-wave 1 still dominates the field but to a lesser extent compared with polar latitudes where QS-wave 1 is

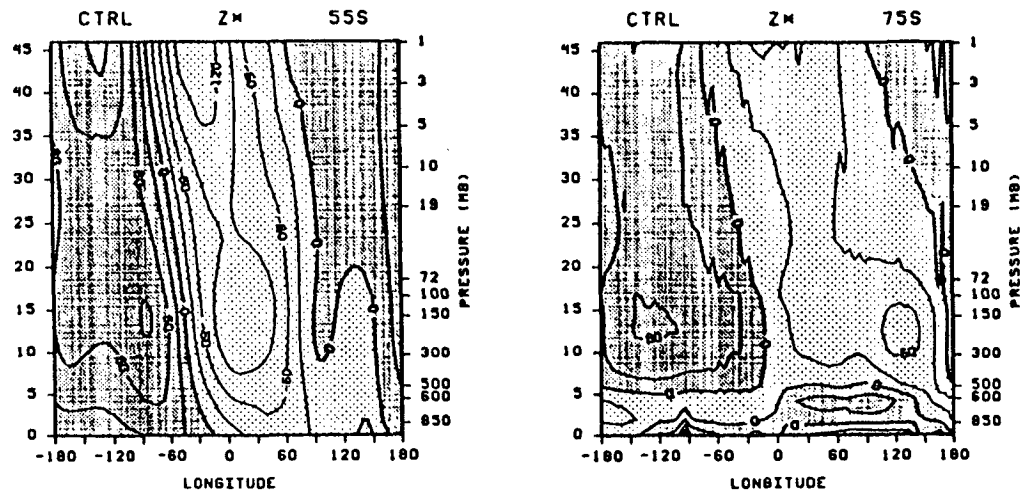


FIG. 3. Height–longitude cross sections for the zonally asymmetric geopotential height at (a) 55°S and 75°S. The contour interval is 15 m.

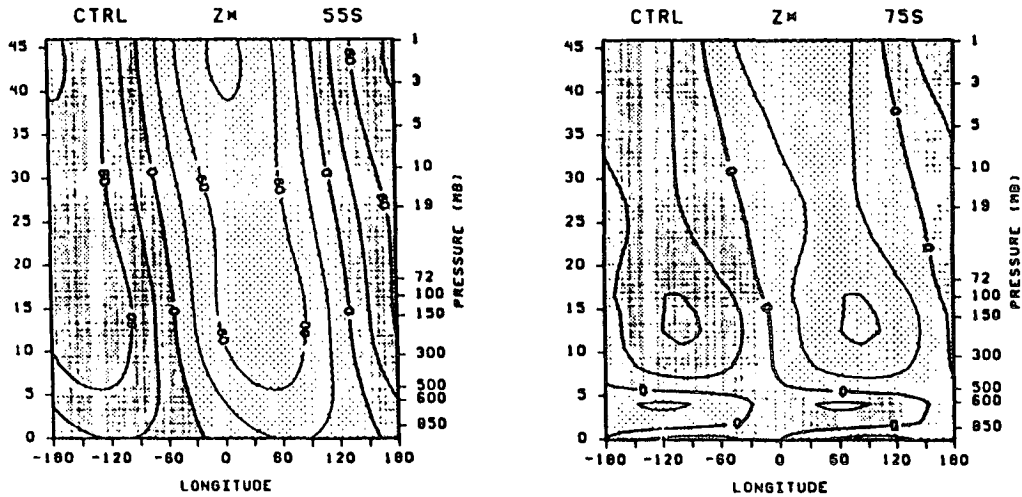


FIG. 4. As in Fig. 3 except for QS-wave 1.

dominant at all levels. QS-wave 1 tilts westward at a rate of about  $2^\circ \text{ km}^{-1}$  at polar latitudes and at about  $1^\circ \text{ km}^{-1}$  in high latitudes. The vertical structure of QS-wave 1 simulated in CTRL is much more equivalent-barotropic than the observed (see Fig. 5 in Part I).

Figure 5 shows the simulated sea level pressure field (SLP) and that compiled from the same NMC dataset used in Part I. The GCM successfully simulates the subtropical highs and to some degree the region of strong meridional pressure gradients at about  $60^\circ\text{S}$ . A somewhat deeper sub-Antarctic trough is simulated at the observed position about  $45^\circ\text{E}$ . However, the simu-

lated field does not clearly show the observed low pressure center over the Ross Sea.

These selected results show that CTRL succeeds in simulating major features of the October circulation in the Southern Hemisphere. In particular, the phase and amplitude of the simulated QS-wave 1 are in close agreement with the observed.

### 3. Hypothesis-testing (H-T) experiments

Our H-T experiments consist of GCM integrations with modified surface conditions. We have performed

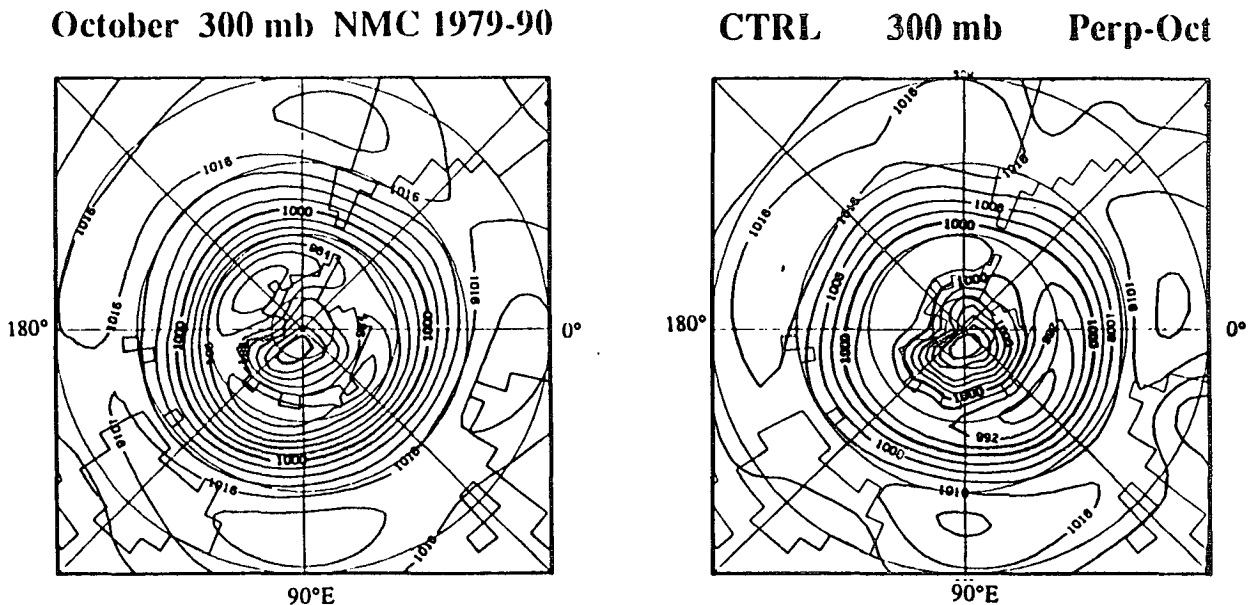


FIG. 5. Sea level pressure fields from the NMC dataset used in Part I (left) and as simulated in the control experiment (right). The contour interval is 4 mb.

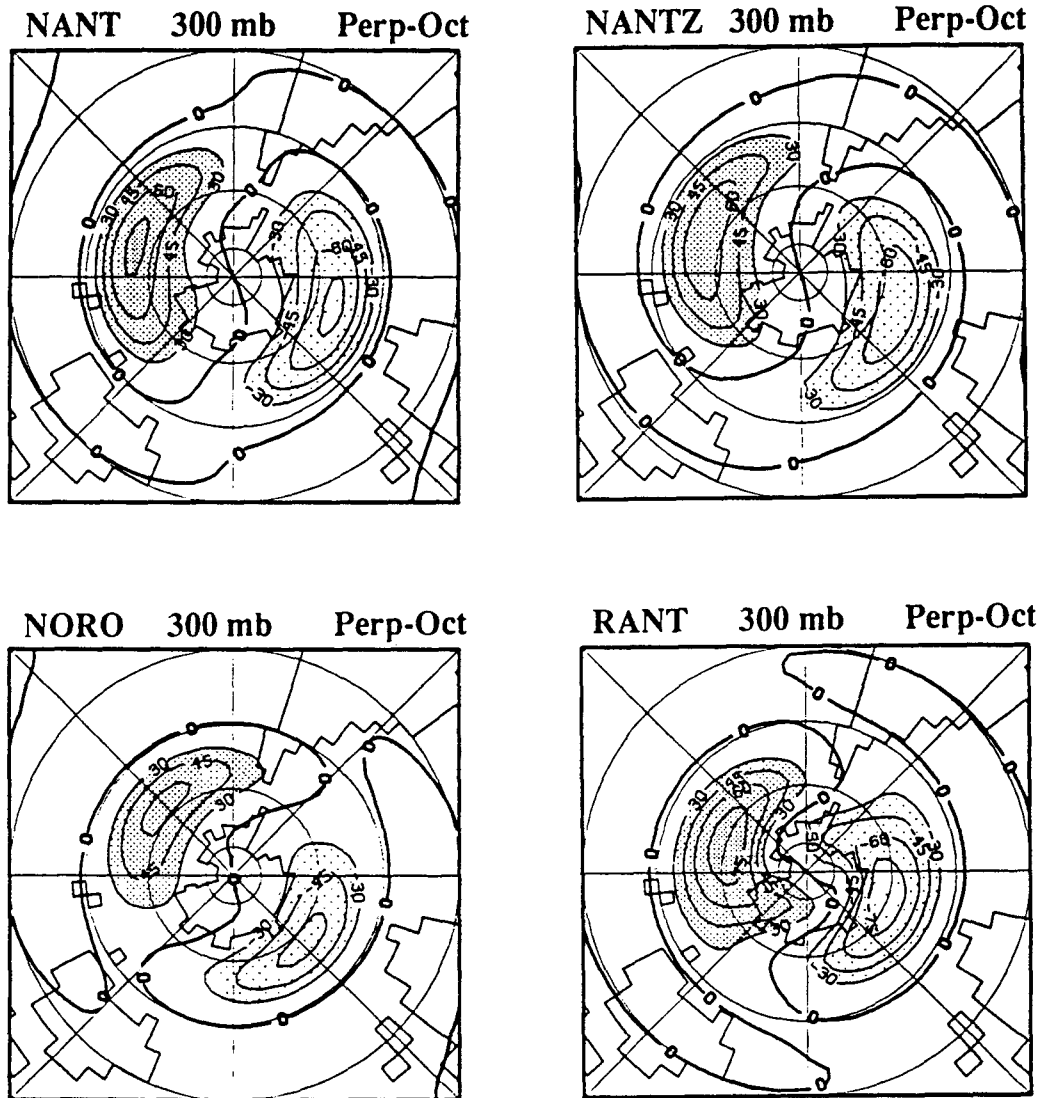


FIG. 6. As in Fig. 2 except for NANT, NORO, NANTZ, and RANT simulations.

several of these experiments: i) NANT, which excludes the Antarctic elevations; ii) NORO, which excludes all orographic elevations; and iii) NANTZ, which excludes all orographic elevations and zonal asymmetries in the surface conditions south of  $45^{\circ}\text{S}$ . For NANTZ, Antarctica and adjacent sea ice were replaced by a shallow circular disk centered at the pole, and of the same combined surface area. Further, the SST was replaced by the zonal average at the corresponding latitude. In NANT and NORO, the SST is the same as in CTRL. To investigate how the quasi-stationary waves are influenced by the zonal asymmetry of the Antarctic continent, an additional H-T simulation was performed with Antarctic elevations rotated  $180^{\circ}$  and all other surface boundary conditions unchanged from that in CTRL (RANT). For the H-T experiments in which orography is artificially modified, the sea level pressure

is required to have the same global mean as in the CTRL simulation so that isobaric heights can be directly compared between different experiments.

Figure 6 shows QS-wave 1 at 300 mb obtained in the H-T experiments. At high latitudes, differences in the phase of QS-wave 1 between H-T experiments are small. QS-wave 1 in NANT, NORO, and NANTZ has a small westward phase shift with respect to that in the CTRL. Over the Antarctic region, QS-wave 1 in NANT, NORO, and NANTZ shows a  $90^{\circ}$  westward phase shift with respect to that obtained in CTRL. Further, QS-wave 1 in RANT and CTRL are almost in opposition of phase as expected.

Figure 7 displays the amplitudes of QS-wave 1 at 300 mb as a function of latitude for October, the control simulation, and the H-T experiments. In the Southern Hemisphere middle and high latitudes, we can see that

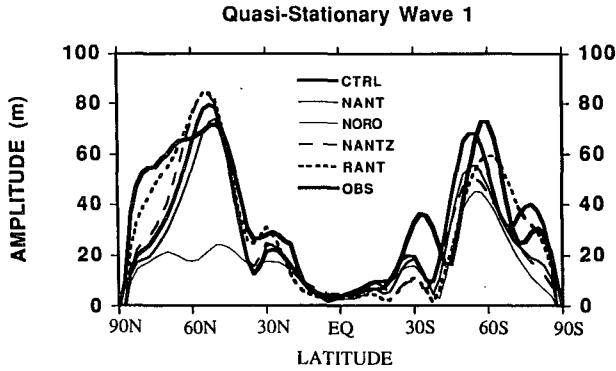


FIG. 7. Amplitude of QS-wave 1 at 300 mb, as a function of latitude for the observed, CTRL, NANT, NORO, NANTZ, and RANT simulations. Units in meters.

none of the artificial modifications made in the GCM boundary conditions have a drastic impact on the simulated QS-wave 1. The amplitudes of QS-wave 1 in NANT and NANTZ are only about 20% to 30% smaller than in the CTRL. The largest and smallest differences with CTRL are obtained in NORO and RANT, respectively. At polar latitudes, the amplitude of QS-wave 1 obtained from observed data shows a local maximum. This is simulated in CTRL, and large magnitudes are also obtained in RANT. The local maximum is absent in all other H-T experiments. In contrast to the Southern Hemisphere, the amplitude of QS-wave 1 in the Northern Hemisphere middle and high latitudes, is about 70% smaller in NORO than in CTRL.

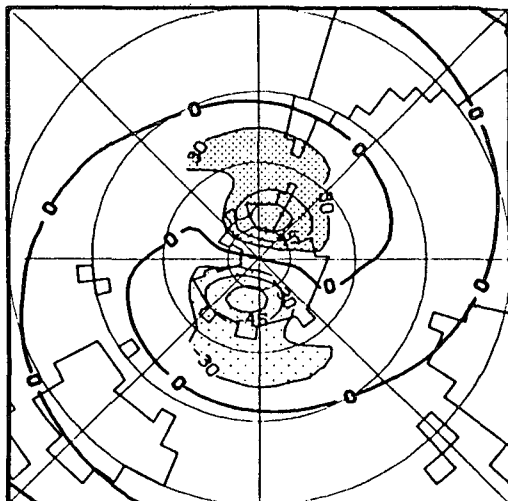
To gain insight into the individual contributions to the quasi-stationary wave field of different elements in the orography, we inspect the differences in QS-wave

1 for CTRL-NANT and CTRL-NORO at 300 mb. These differences can be interpreted, to a first approximation, as the orographic effect of Antarctica and that of all orographic elevations, respectively (see Fig. 8). At high latitudes, CTRL-NANT shows weak negative and positive values over the Australian and South American sectors, respectively. On the other hand CTRL-NORO shows slightly stronger positive and negative values over the Western Pacific and African sectors, respectively. The contrast between CTRL-NANT and CTRL-NORO suggests that the contribution of Antarctica to QS-wave 1 is smaller than that of other orographic elements. At polar latitudes, both CTRL-NANT and CTRL-NORO show a center of negative values over East Antarctica and of positive values over the Antarctic peninsula. Consistent with the results shown in Fig. 7, the effect of Antarctic elevations is most clearly seen at polar latitudes.

The small change in QS-wave 1 amplitude found in the experiments without the Antarctic elevations is in qualitative agreement with the results of Simmonds and Lin (1983). It is also in qualitative agreement with the results obtained by K. Walsh (personal communication) using a version of the Australian Bureau of Meteorology GCM. He found a 30% amplitude reduction for QS-wave 1 at about 50°S and about 50% reduction at about 70°S when the Antarctic elevations in his model are removed. The impact of the Antarctic elevations on the QS-wave 1 field is smaller than expected from simple models, such as barotropic models (e.g., Quintanar and Mechoso 1989) and baroclinic models (e.g., Valdes and Hoskins 1991; Watterson and James 1992).

To estimate the influence of zonal asymmetries in sea ice and SST south of 45° on the quasi-stationary

CTRL-NANT 300 mb Perp-Oct



CTRL-NORO 300 mb Perp-Oct

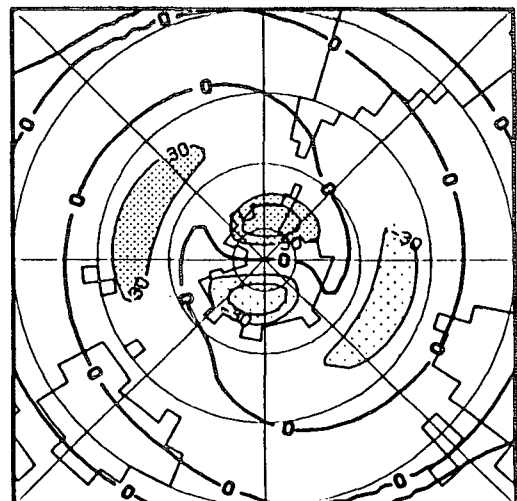


FIG. 8. As in Fig. 4 except for the differences CTRL-NANT (left) and CTRL-NORO (right).

flow field, we inspect the differences in QS-wave 1, 2, and 3 for NANT-NANTZ at 300 mb. The larger magnitudes in these difference maps (see Fig. 9) are found in QS-wave 2 and 3 at high and polar latitudes. The differences in QS-wave 2 for NANT-NANTZ have larger magnitudes than in CTRL-NANT and CTRL-NORO (bottom figures) at high and polar latitudes. This suggests that zonal asymmetries in surface conditions other than orography are crucial in determining the phase and amplitude of QS-wave 2. To further see the extent to which changes in surface boundary conditions are related to the changes at upper levels in QS-wave 2, we inspect the temperature fields at 850 mb for NANT and NANTZ (see Fig. 10). Both patterns are similar in phase and magnitude north of about 50°S. South of this latitude, there is an eastward phase shift at high and polar latitudes. These results suggest the phase of QS-wave 2 at high and polar latitudes is strongly linked to the zonal wavenumber 2 asymmetries in SST and sea ice.

Next we look at the longitude–height vertical cross sections of QS-wave 1 for NANT and NORO at 55°S and 75° in Fig. 11. The vertical structure of QS-wave 1 changes dramatically in the absence of Antarctica at polar latitudes in the troposphere. The phase of QS-wave 1 shifts westward with respect to CTRL by about 90° in both NANT and NORO, which is consistent with the results presented in Fig. 6. The anticyclone that was present in CTRL is now absent. This suggests that without the Antarctic elevations the model atmosphere can not cool as efficiently. Figure 12 shows latitude–height cross sections of zonally averaged temperature for CTRL and the differences CTRL-NANT and CTRL-NORO. There is a substantial warming of about 12°C over the Antarctic surface when the Antarctic elevations are removed in NANT and NORO.

Figure 13 shows the latitudinal distribution of zonally averaged time-mean northward transport of heat by transient eddies at 300 mb for CTRL, NANT, and NORO. In NORO the poleward heat transport is increased by about 10% at high latitudes, and about doubles at polar latitudes in the Southern Hemisphere. This reinforces the idea that the transient eddies are partly responsible for the warming of the atmosphere over Antarctica in NANT and NORO. The heat transport by the quasi-stationary eddies (not shown) is about one order of magnitude smaller than that due to the transients at high latitudes over the Southern Hemisphere. Also this transport is mostly poleward in all cases except for a small region of Antarctica in NANT and NORO. In NANT and NORO, however, the poleward heat transports by the quasi-stationary eddies are reduced significantly with respect to CTRL. Figure 14 shows the zonal average of the poleward heat transport differences CTRL-NANT and CTRL-NORO by the quasi-stationary and transient eddies. The changes in heat transport are generally of the same order of magnitude and are of opposite sign. Although transients

dominate the poleward heat transport in both hemispheres, the reduction in poleward heat transport by the quasi-stationary eddies in the Northern Hemisphere is larger than the increase in poleward heat transport by the transient eddies. In the Southern Hemisphere the opposite is true at high and polar latitudes. Thus at this level, there is a net cooling over the Northern Hemisphere and parts of the Southern Hemisphere and a net warming over high and polar latitudes of the Southern Hemisphere. This is consistent with the result shown in Fig. 12.

The results of these H-T experiments, therefore, suggest that the different behavior of transient and quasi-stationary eddies in the Southern and Northern Hemispheres might be primarily related to different distributions of orography. The impact of the Southern Hemisphere orography is relatively minor compared to that of the Northern Hemisphere, where forced quasi-stationary waves are more efficient in transporting heat poleward than their Southern Hemisphere counterparts.

#### 4. Propagation of quasi-stationary planetary waves

To gain insight into the possibility of remote forcing of QS-wave 1 from lower latitudes we compute the E–P fluxes as in Part I to diagnose the propagation of quasi-stationary waves in the simulated fields. First, we show in Fig. 15 the horizontal structure of the zonal wind component for CTRL, NANT, and NORO at 300 mb. The subtropical jet in CTRL is confined to a region in the subtropics extending eastward from Australia into the eastern Pacific where it peaks with values of about  $30 \text{ m s}^{-1}$ . There is another region of strong westerlies found at middle latitudes over the African sector. Maximum values of zonal wind velocities are found poleward and eastward over the New Zealand region. Thus the GCM succeeds in simulating the jet split over the New Zealand region (see Fig. 8 in Part I).

The horizontal zonal wind distributions in NANT and NORO resemble that obtained in CTRL. In NORO, the core of the subtropical jet appears to be somewhat more elongated than in CTRL. The jet split over the New Zealand region is also more distinct in this simulation. The corresponding meridional vorticity gradients in CTRL, NANT, and NORO are shown in Fig. 16. The patterns shown in this figure closely match those for the zonal wind in CTRL, NANT, and NORO. Except for the Antarctic region, the areas with negative meridional vorticity gradients are reduced compared to the observed. This indicates that the meridional curvature of the simulated zonal wind is not as strong as in the observed data.

Figure 17 displays the horizontal component of the E–P flux vector at 300 mb for CTRL, NANT, and NORO. In CTRL there are four major wavetrains. The first wavetrain extends from the eastern Pacific toward the Atlantic region. Equatorward E–P fluxes over the Atlantic region are also obtained using observational

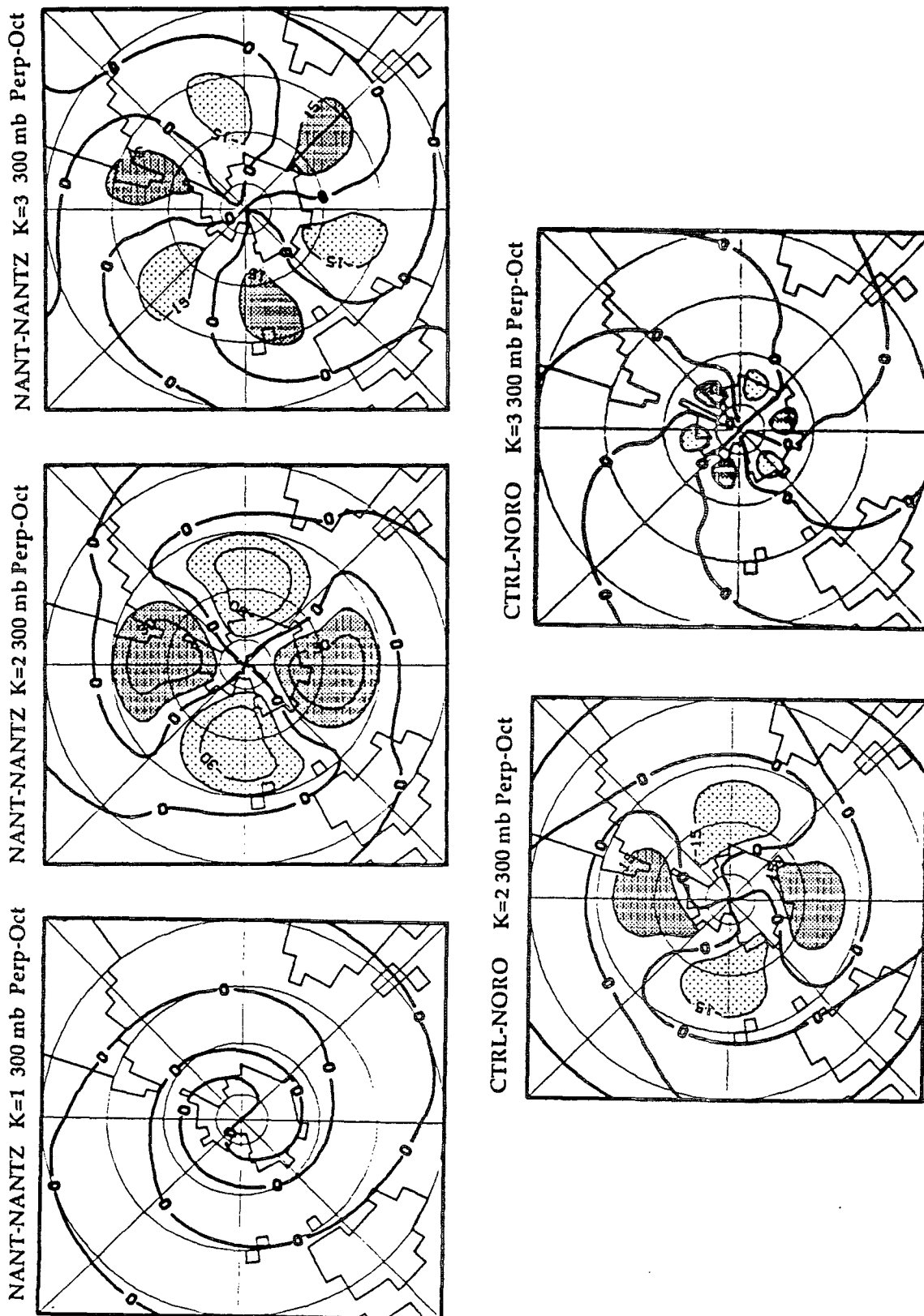


FIG. 9. As in Fig. 2 except for the differences NANT-NANTZ (top) for QS-wave 1 (left), 2 (middle), and 3 (right) and the difference CTRL-NORO (bottom) for QS-wave 2 (left) and 3 (right).

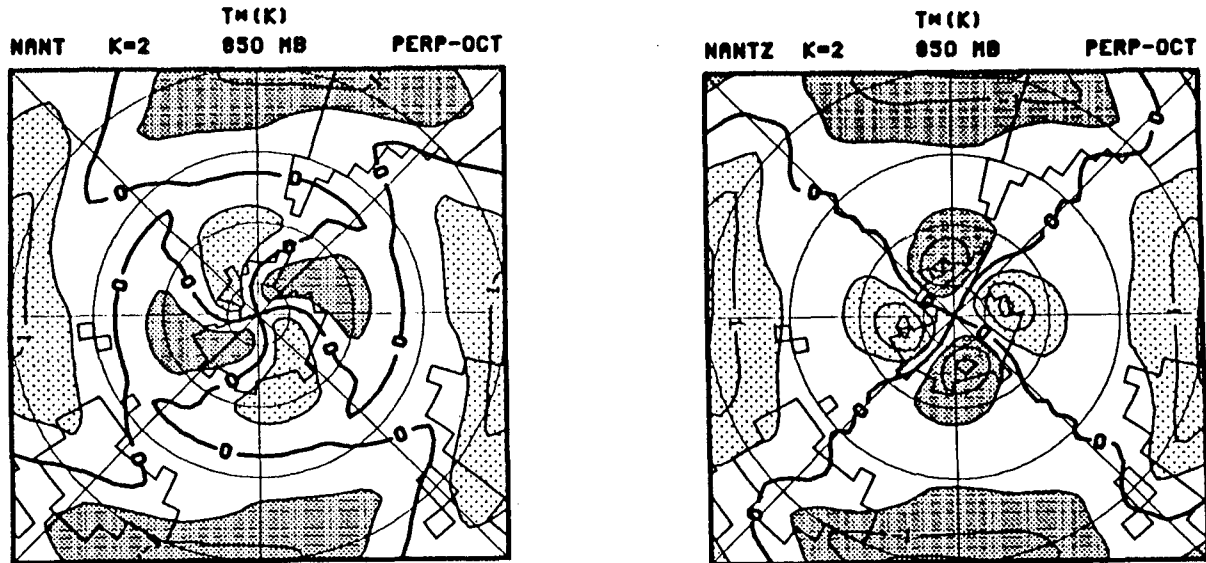


FIG. 10. As in Fig. 2 except for the QS-wave 2 temperature field at 850 mb in the NANT and NANTZ simulations. The contour interval is 0.5 K.

data (see Fig. 10 in Part I), although they are not as distinct as in the simulation. The second wavetrain extends from South Africa toward the Indian Ocean. This feature does not have a clear observational counterpart. A third wavetrain extends from the Australian region toward the central Pacific. This propagation pattern resembles the observed although the simulation does not show a clear connection with the Indian Ocean. A fourth wavetrain appears confined over the Antarctic peninsula region propagating eastward and slightly equatorward. Yang and Gutowski (1994) have studied the propagation of quasi-stationary waves in the GFDL and NCAR general circulation models during the Southern Hemisphere winter. Both models are relatively successful in simulating the observed Indian ocean wavetrain but the simulation at polar latitudes lacks the observed polar wavetrain.

NANT only lacks the polar wavetrain; the source of polar wave activity is clearly associated with the Antarctic elevations and thermal effects. NORO has less intense E–P fluxes, than both CTRL and NANT. Nevertheless, it still shows the wavetrains that extend from the eastern Atlantic region and from the Australian region. These results suggest, therefore, that the latter wave trains partly explain the significant amplitude in simulated QS-wave 1 found at high latitudes of the Southern Hemisphere despite the absence of orography.

##### 5. Effects of large-scale transient eddies on the time-mean flow

In this section we compute the contribution to the quasi-stationary flow at 300 mb by the transient com-

ponent of the flow. The expression used for the vorticity tendency is

$$\frac{\partial \bar{\zeta}}{\partial t} = \mathbf{k} \cdot \nabla \times \mathbf{A}_n, \quad (1)$$

where  $\mathbf{A}_n$  is defined in Part I [see Eqs. (10) and (11)]. Note that the expression (8) in Part I corresponds to an approximation of (1) by assuming geostrophic flow and constant  $f$ . We use vorticity rather than geopotential as in Part I because wind components are provided in the GCM output and were not available in the NMC dataset we used. Figure 18 displays the zonal wave 1 contribution to the quasi-stationary vorticity field by the low-frequency transients for CTRL, NANT, and NORO. Figure 19 displays the corresponding zonal wave 1 for the quasi-stationary vorticity fields. We can see that the meridional scale of the low-frequency contribution of quasi-stationary vorticity is somewhat shorter than the meridional scale of the quasi-stationary fields. At middle and high latitudes, the phase of the contributing terms roughly coincides with the phase of QS-wave 1 vorticity fields for CTRL, NANT, and NORO. Inspection of the time-mean and vorticity forcing fields for CTRL appears to indicate that these two fields are largely anticorrelated and therefore the low-frequency transients in this case tend to damp the time-mean flow. NANT and NORO exhibit a similar situation, except that at polar latitudes (and to some extent in high latitudes) the low-frequency contribution is roughly in phase with the time-mean vorticity field.

Figure 20 shows the high-frequency vorticity contribution to the quasi-stationary vorticity fields in CTRL, NANT, and NORO (note the contour interval here is 20 times smaller than in Fig. 18). Here we use

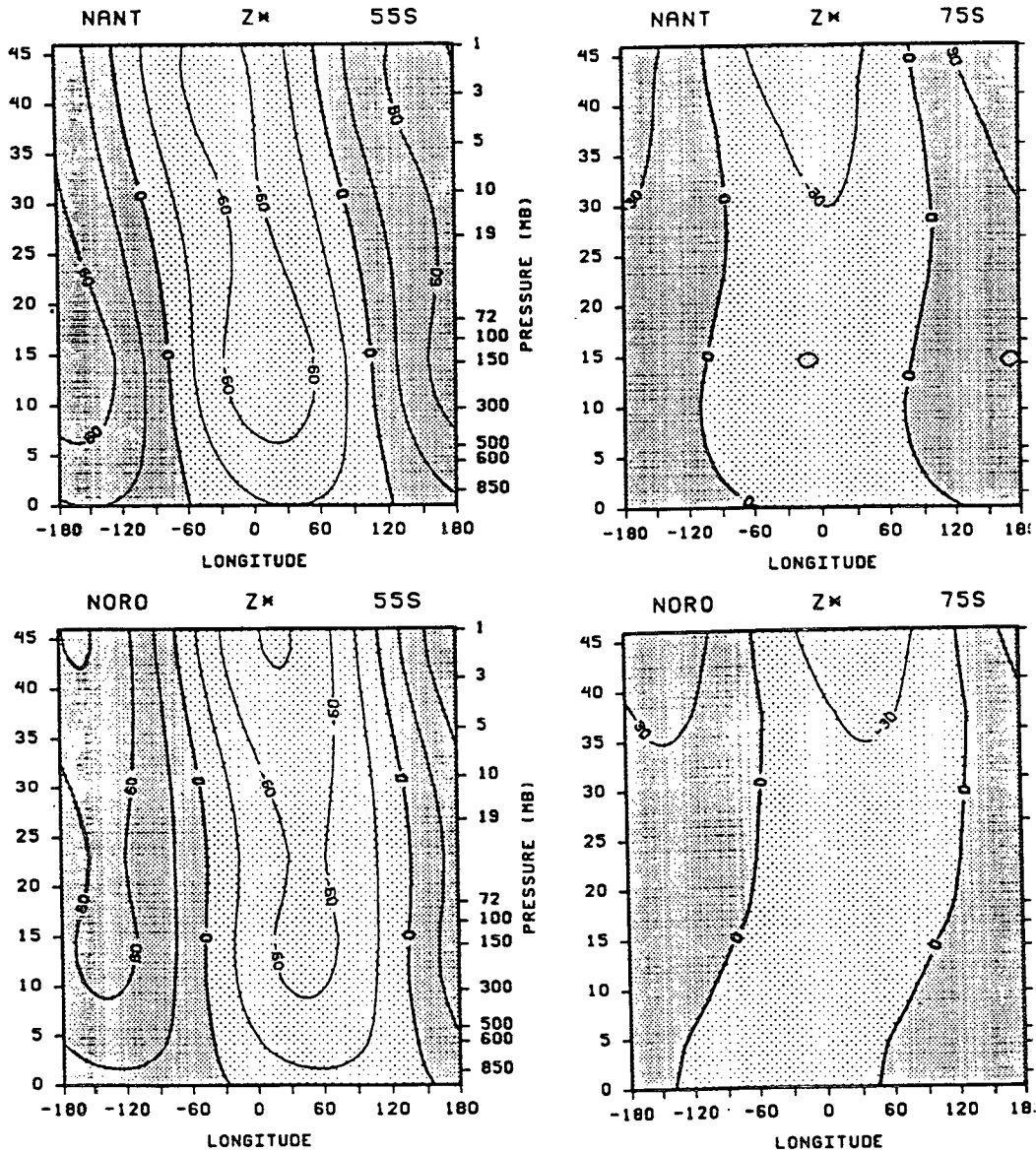


FIG. 11. As in Fig. 4 except for NANT and NORO.

the same cutoff frequency (15 days) as in our observational analysis (Part I). The high-pass transients have a very different horizontal structure and much smaller amplitude than their low-pass counterparts. They all have a broader meridional scale with their phase at almost all latitudes practically unchanged from experiment to experiment. Further, the phase of the high-frequency transients seems to be roughly in quadrature with the phase of the quasi-stationary vorticity fields. We conclude that at polar and high latitudes, the effect of the low-frequency transients in CTRL tends to damp the quasi-stationary flow. When the orographic elevations are removed (NANT and NORO), the effect is to amplify the time-mean flow. The effect of the

high-pass transients is much smaller since the contribution fields and the time-mean fields are practically uncorrelated in space.

The behavior of simulated low-pass and high-pass transients has substantial differences with that estimated from observational data. For instance, the observed high-pass transients have a smaller meridional scale than their low-pass counterparts (not shown). We also concluded earlier (see Part I) that the low-pass transients contribute to the amplification of QS-wave 1, whereas the high-pass transients damp the time-mean flow.

It appears that the main mechanism in our GCM that maintains a substantial QS-wave 1 at high latitudes is

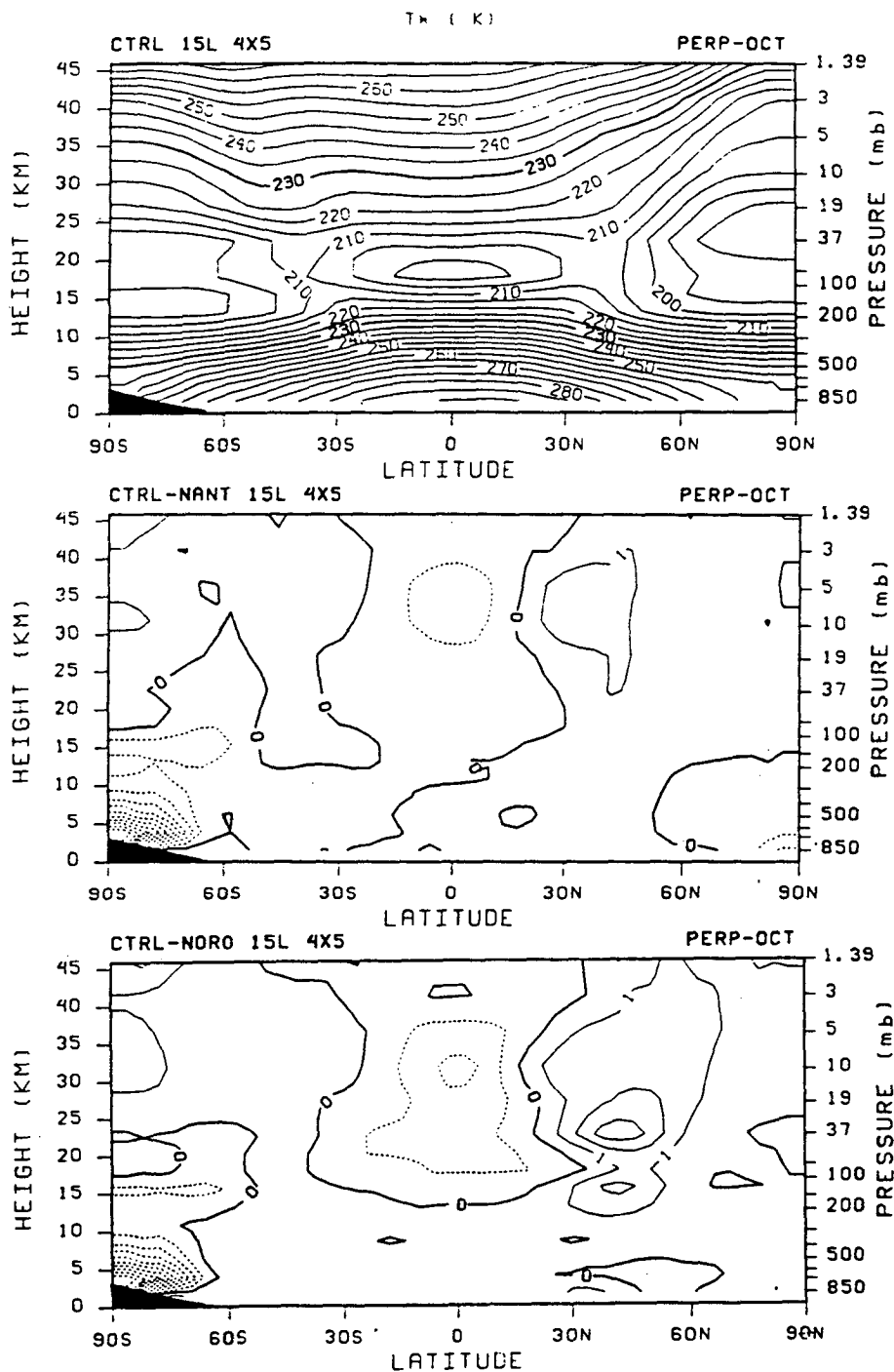


FIG. 12. Height-latitude cross section of the zonally averaged temperature field. Dashed lines correspond to negative values. The contour interval is 5 K for the top panel and 1 K for the two bottom panels.

forcing of wave activity from lower latitudes. The forcing by the transient eddies appears to be smaller in this respect. The reasons for the different behavior exhibited by the transient component of the flow are beyond the scope of this study.

## 6. Summary and conclusions

The objective of this study is to investigate the role that Antarctic elevations, the rest of the world orography, thermal forcing from lower latitudes, and the tran-

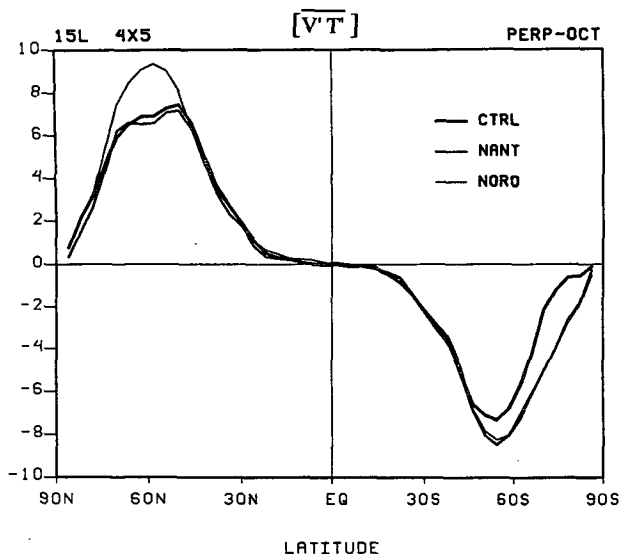


FIG. 13. Zonally averaged meridional heat transport by transient eddies, as a function of latitude at 300 mb. Thick line corresponds to CTRL, medium to NANT, and thin NORO. Units are  $K m s^{-1}$ .

sient eddy component of the flow play on the generation of the quasi-stationary wave field in the Southern Hemisphere. In Part I we presented major features of

the quasi-stationary wave field in the troposphere and stratosphere. In Part II, we followed an approach based on the UCLA GCM.

The results from observational data suggest that the effects of transient eddies and thermal forcing from lower latitudes contribute to enhance the amplitude of the quasi-stationary wave field in the high latitudes of the Southern Hemisphere.

In high latitudes, the simulations performed with the UCLA GCM without the Antarctic orography or even with the Antarctic orography rotated  $180^\circ$  around the South Pole show a QS-wave 1 with substantial amplitude and approximately the same phase as in the control simulation with full orography. At polar latitudes, on the other hand, the local maximum in QS-wave 1 amplitude that is present in the observational data is only obtained in the control simulation, and the experiment where the Antarctic elevations are rotated  $180^\circ$ . The largest decrease (about 40%) in the amplitude of QS-wave 1 was obtained in the experiment with no orographic elevations. We conclude that QS-wave 1 at high latitudes is primarily generated by mechanisms other than the Antarctic elevations. These elevations affect QS-wave 1 at high latitudes, but to a lesser extent and almost in phase with other forcings.

We found that remote forcing of quasi-stationary waves is present in all simulations. At high and middle latitudes, in the control simulation, several wavetrains

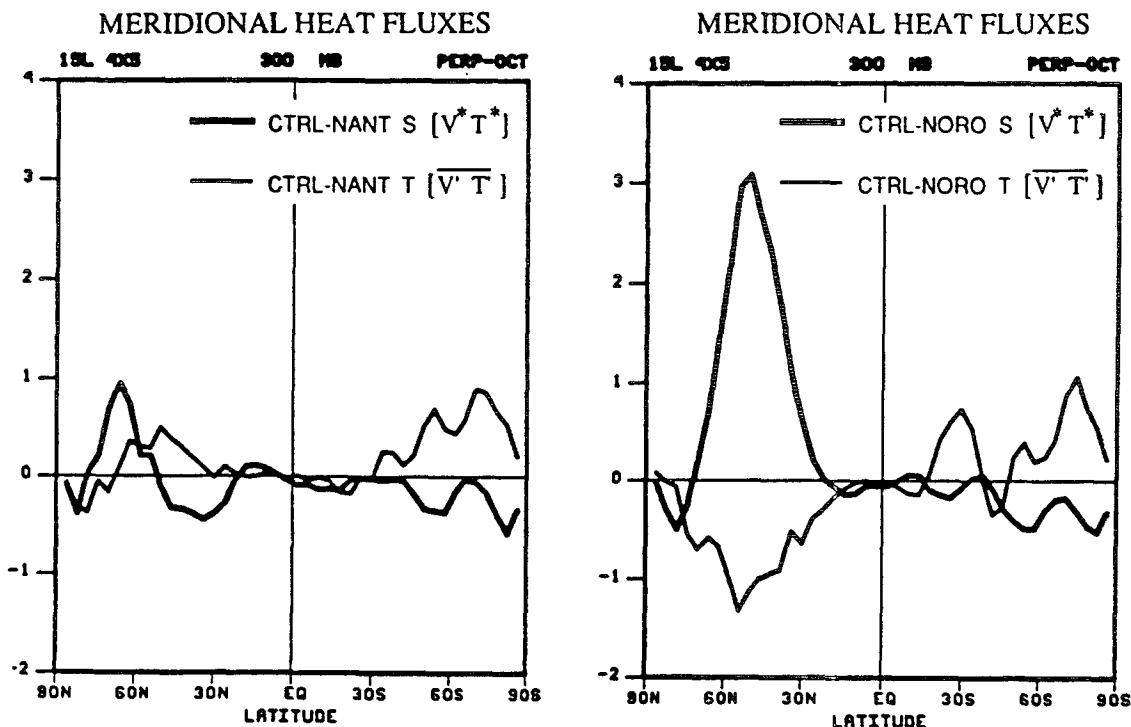


FIG. 14. As in Fig. 13 except for the differences CTRL-NANT and CTRL-NORO for both transient and quasi-stationary waves.

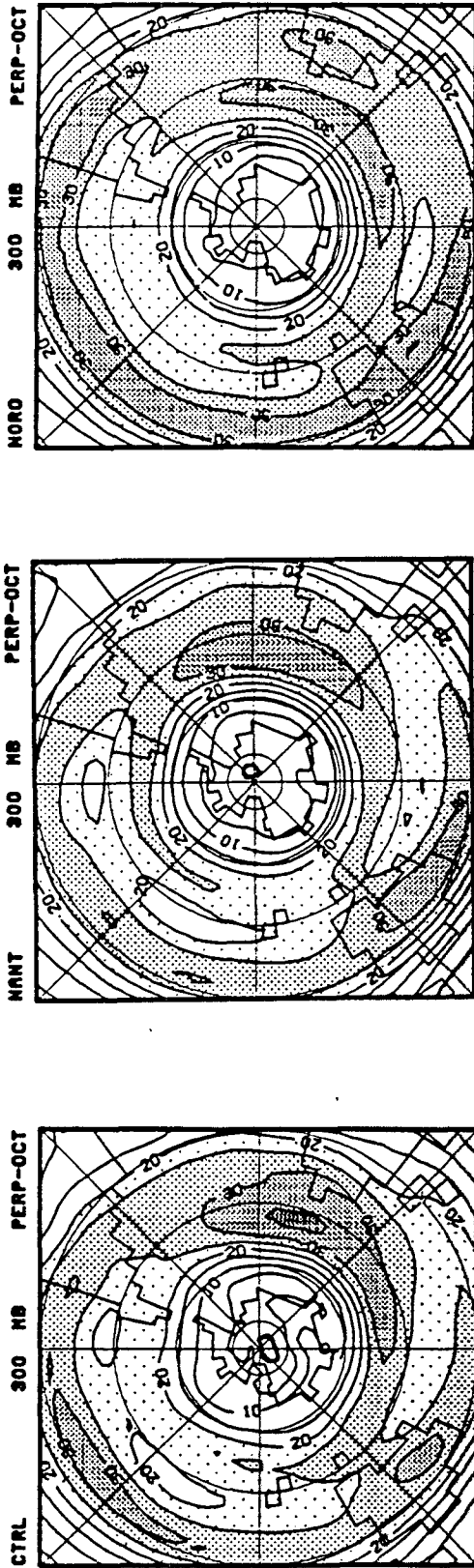


FIG. 15. Time-averaged zonal wind component at 300 mb for CTRL, NANT, and NORO. The contour interval is  $5 \text{ m s}^{-1}$ .

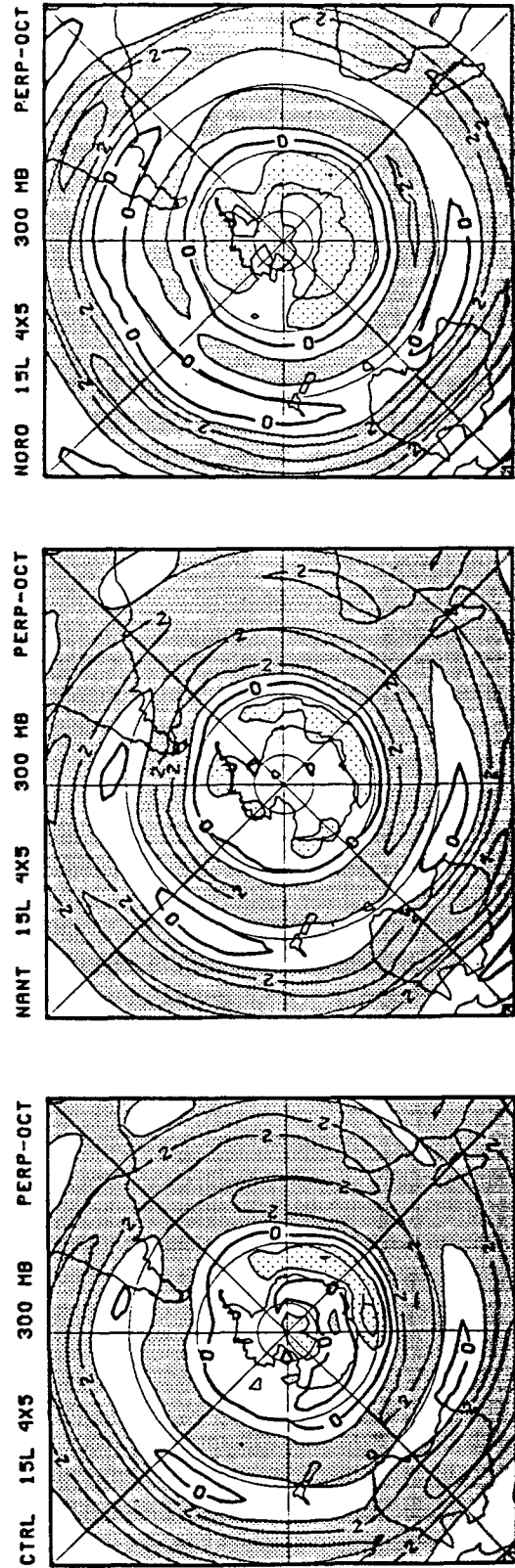
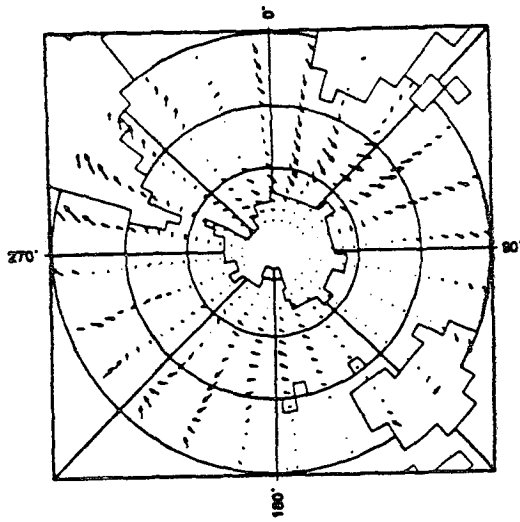
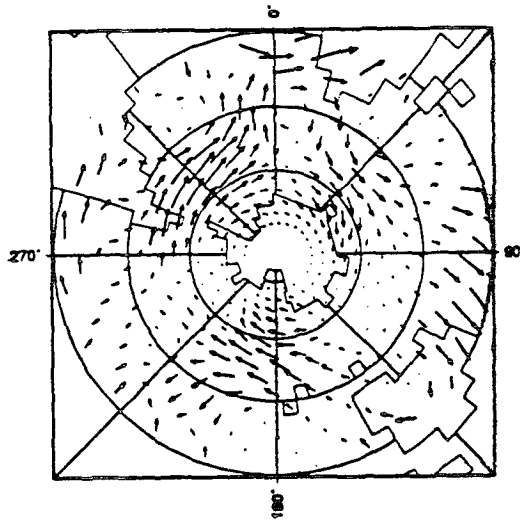


FIG. 16. As in Fig. 15 except for the meridional gradient of absolute vorticity. Contour interval is  $10^5 \text{ m}^{-1} \text{ s}^{-1}$ .

NORO 300 mb EP Flux



NANT 300 mb EP Flux



CTRL 300 mb EP Flux

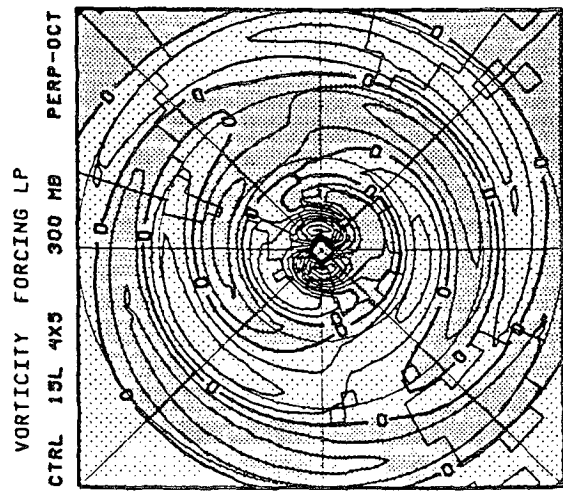
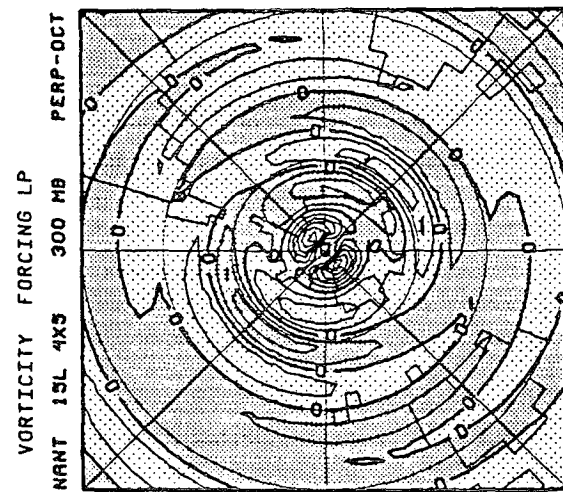
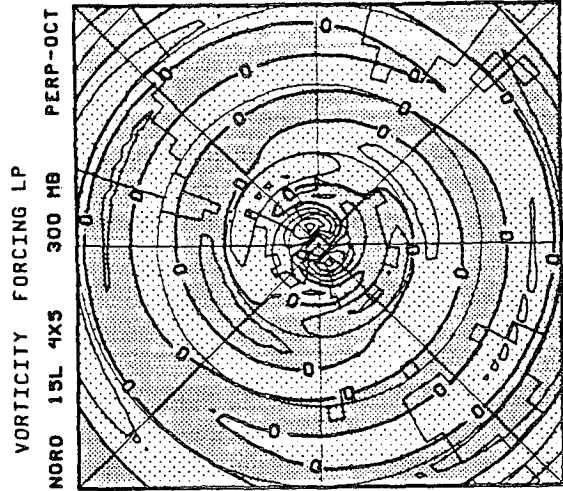
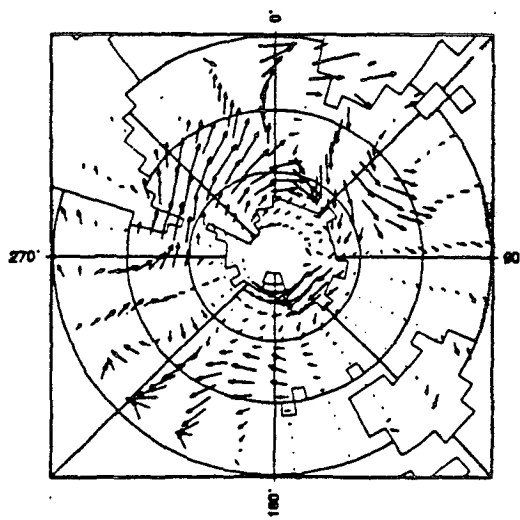


FIG. 17. As in Fig. 15 except for the horizontal E-P flux vector.

FIG. 18. As in Fig. 15 except for the vorticity forcing by the low-frequency eddies. The contour interval is  $1 \cdot 10^5 \text{ s}^{-2}$ .

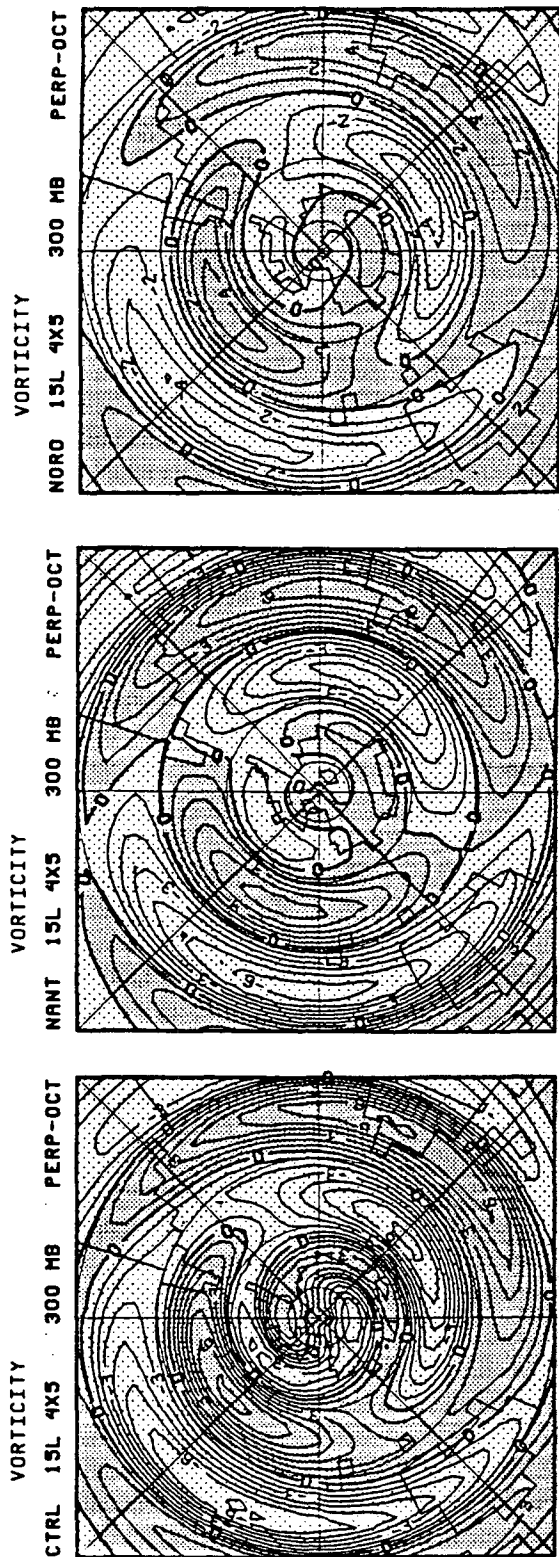


FIG. 19. As in Fig. 15 except for the time-mean vorticity field. The contour interval is  $1 \times 10^6 \text{ s}^{-1}$ .

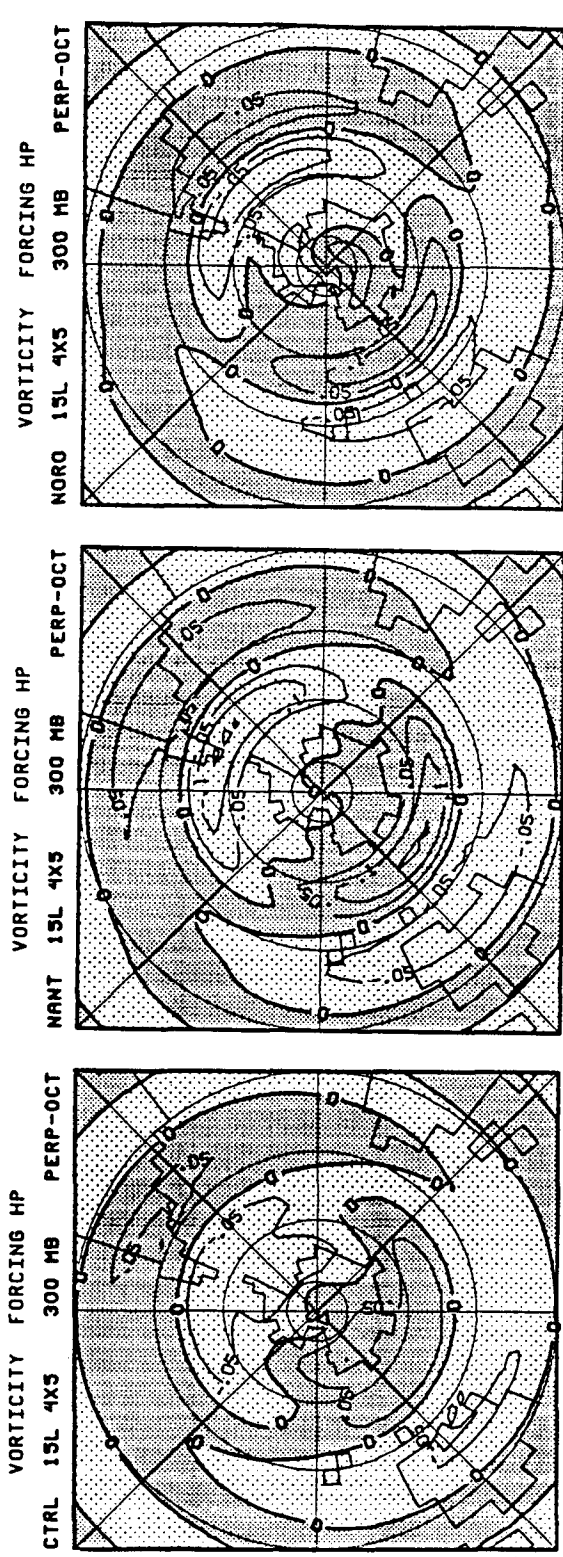


FIG. 20. As in Fig. 18 except for the high frequency eddies. The contour interval is  $0.05 \times 10^5 \text{ s}^{-2}$ .

with an equivalent barotropic structure appear to emanate from the sub-Tropics. At polar latitudes, wave activity propagates eastward and slightly northward close to the Antarctic periphery. As mentioned earlier, this polar wavetrain is an observed feature in winter and spring but unlike the observations, the wavetrain in the GCM seems to be confined to polar latitudes perhaps due to the rather large zonal wind components in the control simulation, which may inhibit meridional and vertical wave propagation.

When the Antarctic elevations are removed this polar wavetrain disappears while the rest of the previous wavetrains remain. When all orographic elevations are removed a wavetrain common to all the experiments propagates from the west coasts of South Africa poleward and eastward and is deflected toward lower latitudes at high latitudes where the amplitude of QS-wave 1 is largest. We conclude that the substantial QS-wave 1 amplitude that remains when all orographic elevations are removed is partly generated by remote forcing from lower latitudes in qualitative agreement with the results of Part I. Future studies will have to address the origin of this low-latitude forcing.

Additional evidence of thermal forcing was found in the simulation without orographic elevations and zonal asymmetries south of 45°S. This simulation shows a QS-wave 2 that has clear differences with the control simulation. The results suggest that these asymmetries are closely linked to the phase of QS-wave 2 at upper levels at high and polar latitudes of the Southern Hemisphere.

The lack of vertical wave propagation in the control simulation is consistent with the mostly barotropic vertical structure of the simulated quasi-stationary waves. This is, at least in part, due to errors in the simulated zonal wind in the upper troposphere (Mechoso et al. 1987). This behavior is different from the observed vertical propagation of quasi-stationary waves in October. It is not clear at present why our GCM produces such a different pattern of horizontal and vertical wave propagation. The suggestion seems to be that the horizontal distribution of tropical convective activity is also different. Further analysis of the observed and simulated heating distributions needs to be done to determine this precisely.

Analysis of the contribution of the quasi-stationary flow by the low-pass transients in the control simulation shows that they are out of phase with respect to QS-wave 1. When orographic elevations are removed, the phase of the low-pass transients is similar to QS-wave 1 in polar and high latitudes. The contribution by the high-pass transients is smaller since their phases are almost in quadrature with that of QS-wave 1 in all simulations.

Antarctica plays an important role in maintaining the low South Polar temperatures. We found an enhancement of poleward heat transport by the transient eddies in the absence of Antarctic elevations consistent with

warming of the Antarctic region. Concurrent with this, the heat transports by the stationary eddies is reduced by similar orders of magnitude. Mechoso (1981) suggested that this effect is associated with the different behaviors of the synoptic-scale transient eddies. In his scenario, the polar region warms partly because cyclones can translate further poleward after the constraints on their trajectories imposed by Antarctic elevations are removed.

It appears that the main mechanism in our GCM that maintains a substantial QS-wave 1 at high latitudes is forcing of wave activity from lower latitudes. The contribution by the transient component appears to be smaller.

Can our results be reconciled with those obtained by using idealized models? To answer this question we consider that those models also include idealized forcings, whose intensity depends on "tunable" coefficients. There is, therefore, some degree of ambiguity in the results since the values of the coefficients may be selected to produce realistic amplitudes in a feature of interest, and this feature is strongly influenced by processes not included in the idealized model. We are of the opinion that these considerations are particularly appropriate in the case of the Antarctic influence on the atmospheric circulation. Specifically, the barotropic response to Antarctica is one component, albeit not the most important, in the circulation at the high latitudes of the Southern Hemisphere. The ambiguity arises as the barotropic component of the response to Antarctica only has a relatively small difference in phase with the response to forcings from low latitudes.

*Acknowledgments.* We are grateful to J. Farrara for providing the data for this study and to J. Spahr for helping with the GCM data. Ms. C. Wong and Ms. K. Hartman typed the manuscript. This research was supported by NSF ATM-8814892 and ATM-9122153, and by CalSpace under Grant CS-25-88.

#### APPENDIX A

##### The UCLA General Circulation Model

The UCLA GCM is based on the primitive equations. The model's prognostic variables are the horizontal velocity, potential temperature, water vapor mixing ratio, ozone mixing ratio, surface pressure, planetary boundary layer (PBL) depth, and ground temperature. Formulation of the diabatic processes include parameterizations of cumulus convection (Arakawa and Schubert 1974), PBL processes (Suarez et al. 1983), and a radiation calculation (Katayama 1972). The geographical distributions of surface albedo, ground wetness, sea surface temperature (SST), and sea ice are interpolated from prescribed monthly means based on the observed climatology. Details on the GCM are given in Mechoso et al. (1987) and references therein. In this study, we use the 15-layer ver-

sion, which has the top at 1 mb (about 45 km) and six layers above 51.8 mb. This choice is based on our interest to study planetary-scale waves, whose behavior can be strongly affected by a lower upper boundary (Mechoso et al. 1987). Monthly mean fields from long-term simulations with the GCM have been evaluated by Suarez et al. (1983) and Randall et al. (1985).

## REFERENCES

- Arakawa, A., and W. H. Schubert, 1974: Interaction of a cumulus cloud ensemble with the large-scale environment. Part I: *J. Atmos. Sci.*, **31**, 674–701.
- Charney, J. G., and A. Eliassen, 1949: A numerical method for predicting the perturbations of the middle latitude westerlies. *Tellus*, **1**, 38–54.
- Dickinson, R. E., 1980: Planetary waves: Theory and observation. *Orographic Effects in Planetary Flows*, GARP Publication Series No. 23, WMO-ICSU, 53–84.
- Held, I. M., 1983: Stationary and quasi-stationary eddies in the extratropical troposphere: Theory. *Large-Scale Dynamical Processes in the Atmosphere*, B. J. Hoskins and R. P. Pearce, Eds., Academic Press, 127–168.
- James, I. N., 1988: On the forcing of planetary-scale Rossby waves by Antarctica. *Quart. J. Roy. Meteor. Soc.*, **114**, 619–637.
- Jenne, R. L., H. L. Crotcher, H. van Loon, and J. S. Taljaard, 1974: A selected climatology of the Southern Hemisphere: Computer methods and data availability. NCAR-TN STR 92, NCAR, Boulder, CO., 91 pp.
- Kasahara, A., 1980: Influence of orography on the Atmospheric General Circulation. Orographic effects in planetary flows, GARP Publication Series No. 23, WMO, Geneva, 4–49.
- Katayama, A., 1972: A simplified scheme for computing radiative transfer in the troposphere. *Numerical Simulation of Weather and Climate*, Tech. Rep. No. 6. Dept. Meteorology, University of California, Los Angeles, 77 pp.
- Mechoso, C. R., 1981: Topographic influences on the general circulation of the Southern Hemisphere: A numerical experiment. *Mon. Wea. Rev.*, **109**, 2131–2139.
- , A. Kitoh, S. Moorthi, and A. Arakawa, 1987: Numerical Simulations of the atmospheric response to a sea surface temperature anomaly over the equatorial eastern Pacific Ocean. *Mon. Wea. Rev.*, **115**, 2936–2956.
- Quintanar, I. A., and C. R. Mechoso, 1989: Generation mechanisms of quasi-stationary waves in the Southern Hemisphere. *Extended Abstracts, Third Int. Conf. on the Southern Hemisphere Meteorology and Oceanography*, Buenos Aires, Argentina, American Meteorological Society, 271–274.
- Randall, D. A., J. A. Abeles, and T. G. Corsetti, 1985: Seasonal simulations of the planetary boundary layer and boundary layer stratocumulus clouds with a general circulation model. *J. Atmos. Sci.*, **42**, 641–676.
- Simmonds, I., and Y. Lin, 1983: Topographical and thermal forcing in a circulation model of the Southern Hemisphere. January case. The University of Melbourne, Meteorology Department, Publication No. 24.
- Smagorinsky, J., 1953: General Circulation experiment with the primitive equations. Part I: The basic experiments. *Mon. Wea. Rev.*, **91**, 99–164.
- Smith, R. B., 1979: The influence of mountains on the atmosphere. *Advances in Geophysics*, Vol. 21, Academic Press, 87–230.
- Suarez, M. J., A. Arakawa, and D. A. Randall, 1983: The parameterization of the planetary boundary layer in the UCLA general circulation model: Formulation and results. *Mon. Wea. Rev.*, **111**, 2224–2243.
- Tokioka, T., and A. Noda, 1986: Effects of large-scale orography on the January atmospheric circulation: A numerical experiment. *J. Meteor. Soc. Japan*, **606**, 819–839.
- Valdes, P. J., and B. J. Hoskins, 1991: Nonlinear orographically forced planetary waves. *J. Atmos. Sci.*, **48**, 2089–2106.
- Watterson, I. G., and I. N. James, 1992: Baroclinic waves propagating from a high latitude source. *Quart. J. Roy. Meteor. Soc.*, **118**, 23–50.
- Yang, S., and W. J. Gutowski Jr., 1994: GCM Simulations of the three-dimensional propagation of stationary waves. *J. Climate*, **7**, 414–432.